Stable Delocalized Singlet Biradical Hydrocarbon for Organic Field-Effect Transistors

Harunobu Koike, Masayuki Chikamatsu, Reiko Azumi, Jun'ya Tsutsumi, Kazumichi Ogawa, Wataru Yamane, Tomohiko Nishiuchi, Takashi Kubo, Tatsuo Hasegawa, and Kaname Kanai*

Delocalized singlet biradical hydrocarbons hold promise as new semiconducting materials for high-performance organic devices. However, to date biradical organic molecules have attracted little attention as a material for organic electronic devices. Here, this work shows that films of a crystallized diphenyl derivative of *s*-indacenodiphenalene (Ph_2-IDPL) exhibit high ambipolar mobilities in organic field-effect transistors (OFETs). Furthermore, OFETs fabricated using Ph_2-IDPL single crystals show high hole mobility ($\mu_h = 7.2 \times 10^{-1}$ cm^2 V^{-1} s^{-1}) comparable to that of amorphous Si. Additionally, high on/off ratios are achieved for Ph_2-IDPL by inserting self-assembled monolayer of alkanethiol between the semiconducting layer and the Au electrodes. These findings open a door to the application of ambipolar OFETs to organic electronics such as complementary metal oxide semiconductor logic circuits.

1. Introduction

Electrical properties of a molecular solid can be strongly influenced by its purity and quality, for example, the carrier mobility of organic solid is readily decreased by the presence of defects and impurities. Consequently, high-performance organic electronic devices require the use of single crystals free of defects and impurities as much as possible.

There have been reports over the last decade that organic single crystals such as rubrene and pentacene exhibit high carrier mobility comparable to that of amorphous Si,[1,2] but the electrical properties of these organic crystals remain inferior to those of conventional inorganic semiconductor crystals. In most organic semiconductors, including rubrene and pentacene, the crystal is condensed through weak, short-range dispersion forces. Highly coherent energy band transport observed in inorganic semiconductor single crystals is unlikely in organic crystals because the overlapping of the π-orbitals is quite small due to the very weak intermolecular interactions between organic molecules. Consequently, strong intermolecular interactions are desirable to obtain high carrier mobility comparable to that of inorganic semiconductor crystals.

The molecules in some organic semiconductors aggregate by dipole–dipole or dipole-induced dipole interactions, which are stronger than dispersion forces. For example, *p*-iodobenzonitrile crystal contains strong nitrogen–iodide (N–I) contacts, providing a 1D molecular chain. The N–I distance (3.18 Å) is shorter than the van der Waals contact distance (3.65 Å).[3,4] Charge transfer interaction is also stronger than dispersion forces. bis(1,2,5-thiadiazolo)-*p*-quinobis(1,3-dithiole) (BTQBT) shows high conductivity comparable to that of Ge as a result of charge transfer interactions; in addition, it is considered that the properties of BTQBT crystals are described by their band transport properties.[5,6] Some effort has been made to take advantage of these strong intermolecular interactions to obtain high-mobility devices.

Organic radicals with an unpaired electron exhibit strong inter-radical covalent interactions. A half-filled orbital in an organic radical appears to guarantee metal-like electrical properties. However, on-site Coulomb interactions between the unpaired electrons maintain the semiconducting properties of the organic radical crystal. Moreover, many organic radicals suffer from a serious disadvantage: they are chemically unstable in air. These radicals tend to dimerize and the carriers localize at one site.

The generation of stable radicals exhibiting high electrical conductivity has been investigated. Recently, a biradical molecule, which contains two radical moieties in the molecules, has been synthesized as a new type of semiconductor material for electronic devices.[7–13] The diphenyl derivative of *s*-indacenodiphenalene (Ph_2-IDPL) (**Figure 1**a) is a stable delocalized singlet biradical hydrocarbon and is of particular interest. Ph_2-IDPL

H. Koike, K. Ogawa, W. Yamane, Prof. K. Kanai
Department of Physics
Tokyo University of Science
2641 Yamazaki, Noda, Chiba 278-8510, Japan
E-mail: 6214701@ed.tus.ac.jp
Dr. M. Chikamatsu, Dr. R. Azumi, Dr. J. Tsutsumi, Prof. T. Hasegawa
National Institute of Advanced Industrial Science and Technology (AIST)
AIST Tsukuba Central 5, 1-1-1 Higashi, Tsukuba, Ibaraki 305-8565, Japan
Prof. T. Nishiuchi, Prof. T. Kubo
Department of Chemistry
Osaka University
1-1 Machikaneyama, Toyonaka, Osaka 560-0043, Japan
Prof. T. Hasegawa
Department of Applied Physics
The University of Tokyo
7-3-1 Hongo, Bunkyo-ku, Tokyo 113-8656, Japan

DOI: 10.1002/adfm.201503650

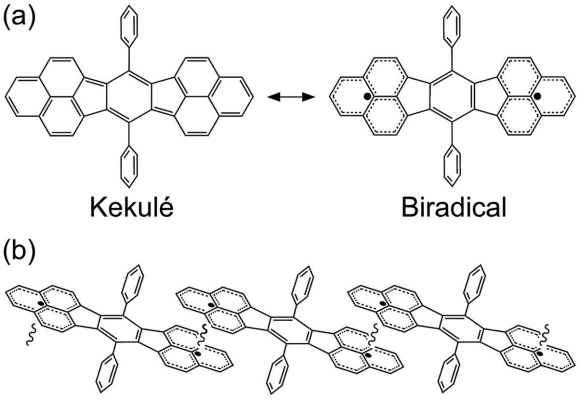

Figure 1. a) Chemical structure of Ph_2-IDPL. Ph_2-IDPL can be drawn by the resonance structure between the Kekulé and biradical structures. b) A quasi-1D molecular chain of Ph_2-IDPL. Wavy lines represent intermolecular interactions.

has two phenalenyl radical structures, one at each end of the molecule. The dominant attractive force between Ph_2-IDPL molecules originates from the bonding interactions between the radical structures. In the crystal, Ph_2-IDPL molecules form a quasi-1D molecular chain in a slipped stacking arrangement (Figure 1b).[14] We previously reported that the Ph_2-IDPL crystallized film has a small energy gap between the highest occupied molecular orbital (HOMO) and the lowest unoccupied molecular orbital (LUMO), and a large π-band dispersion of around 1 eV.[15,16] Organic field-effect transistors (OFETs) based on a Ph_2-IDPL amorphous film exhibit balanced hole and electron mobilities (hole mobility $\mu_h = 2.6 \times 10^{-3}$ cm^2 V^{-1} s^{-1}, electron mobility $\mu_e = 3.2 \times 10^{-3}$ cm^2 V^{-1} s^{-1}).[17] It has been believed that the electrical property of OFET is governed by the injection at the electrode interface. In the case of the amorphous Ph_2-IDPL film, the OFETs show ambipolar behavior because both HOMO and LUMO are close to the Fermi level (E_F) of electrode. However, the OFETs using an amorphous film cannot take advantage of the above-mentioned strong intermolecular interactions between Ph_2-IDPL molecules. Ph_2-IDPL single crystals should exhibit ambipolar properties with high mobilities due to large π-band dispersion arising from the strong intermolecular interactions. Therefore, we focus on the electronic structure and electrical properties of a highly crystallized Ph_2-IDPL film and Ph_2-IDPL single crystals. To date, biradical organic molecules have attracted little attention as materials for organic electronic devices partly due to their chemical instability. However, this work reveals that Ph_2-IDPL has excellent electrical properties comparable to those of amorphous Si. Our findings indicate that delocalized singlet biradical hydrocarbons are promising as new semiconducting materials for high-performance organic devices because of its singlet biradical nature.

2. Development of Electronic Structure

There is a close relationship between the electrical properties of OFETs and the electronic structure of an organic semiconductor. Ph_2-IDPL films with different crystallinities have significantly different electronic structures. Therefore, the electrical

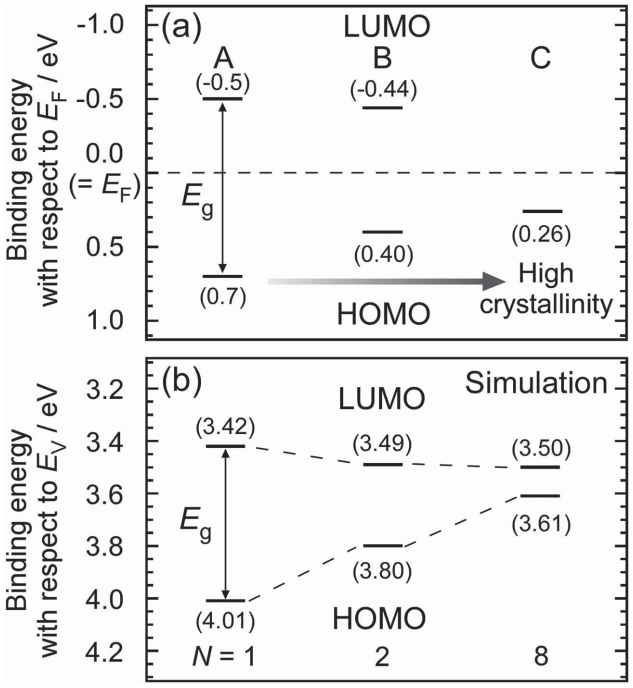

Figure 2. a) HOMO and LUMO energy diagram of Ph_2-IDPL films. HOMO and LUMO energy levels were measured by UPS and IPES, respectively. Ph_2-IDPL films were in an amorphous state (A), a polycrystalline state (B), and a polycrystalline state with higher crystallinity (C).[15,16] The vertical axis indicates binding energy with respect to the Fermi level (E_F). E_g indicates the energy gap between HOMO and LUMO. b) Simulated HOMO and LUMO levels calculated by DFT for Ph_2-IDPL monomer and oligomers. *N* represents the number of molecules. DFT calculations were performed using the GAUSSIAN 09 package at the PW91/6-31G* level. The vertical axis indicates the binding energy with respect to the vacuum level (E_V).

properties of OFETs fabricated from Ph_2-IDPL films depend on the crystallinity of the film. **Figure 2**a shows the HOMO and LUMO energy diagram of Ph_2-IDPL films deposited in ultrahigh vacuum on graphite (A), deposited in a dry nitrogen atmosphere at $P_{N2} \approx 0.1$ kPa on graphite (B),[15] and deposited in a dry nitrogen atmosphere at $P_{N2} \approx 0.5$ kPa on GeS (C).[16] HOMO and LUMO energy levels were measured by ultraviolet photoemission spectroscopy (UPS) and inverse photoemission spectroscopy (IPES), respectively. The labels A, B, and C designate different crystallinities: A is in an amorphous state, B is in a polycrystalline state, and C is in a polycrystalline state exhibiting higher crystallinity and a large π-band dispersion of around 1 eV. The HOMO levels labeled A, B, and C are $E_{HOMO}{}^A = 0.7$ eV, $E_{HOMO}{}^B = 0.40$ eV, and $E_{HOMO}{}^C = 0.26$ eV, respectively. The HOMO–LUMO gaps labeled A and B are $E_g{}^A = 1.2$ eV and $E_g{}^B = 0.84$ eV, respectively.[15,16] It therefore appears that as the crystallinity becomes higher, the HOMO level shifts toward the E_F and the HOMO–LUMO gap becomes smaller. Figure 2b shows simulated HOMO and LUMO levels calculated by density functional theory (DFT) for Ph_2-IDPL monomer and oligomers ($N = 1, 2, 8$), where *N* indicates the number of molecules. For the calculation, the chemical structures of Ph_2-IDPL monomer and oligomers are taken from results of a single crystal X-ray structure analysis of a Ph_2-IDPL

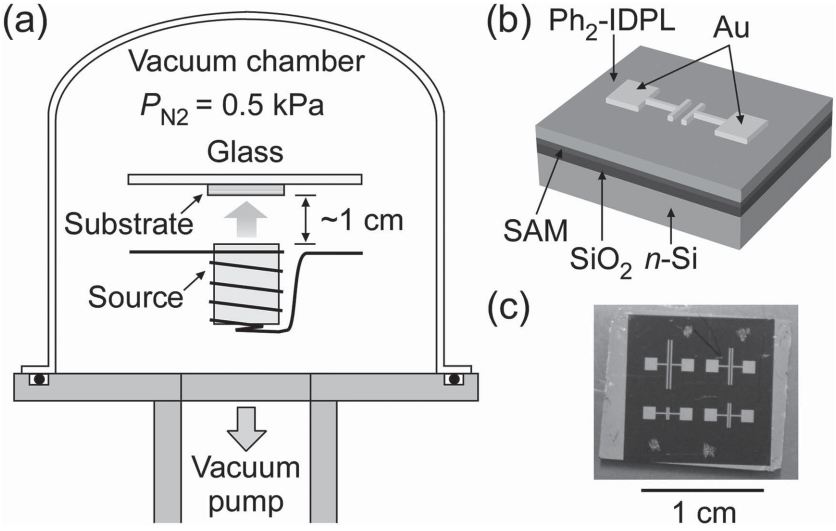

Figure 3. a) Schematic drawing of the gas deposition method. Ph_2-IDPL was deposited on the substrates in a dry nitrogen atmosphere at $P_{N2} \approx 0.5$ kPa in a vacuum chamber. b) Schematic drawing of a top-contact bottom-gate OFET with a Ph_2-IDPL film. HMDS SAM and phenyltrichlorosilane SAM were used. c) Photograph of the OFET. There are four types of electrodes (l/w = 40 μm/1 mm, 80 μm/2 mm, 120 μm/3 mm, and 160 μm/4 mm).

single crystal.[14] As the number of molecules increases, the HOMO level shifts to lower binding energy and the LUMO level shifts to higher binding energy. Thus, the HOMO–LUMO gap becomes smaller. These shifts are induced by the development of the band structure. Therefore, the simulated results overall show good agreement with the experimental results. These results indicate that highly crystallized Ph_2-IDPL film and Ph_2-IDPL single crystal have long Ph_2-IDPL molecular chains. Moreover, these results imply that they have developed band dispersion width and a small HOMO–LUMO gap. And the small HOMO–LUMO gap indicates that OFETs with a highly crystallized Ph_2-IDPL film or a Ph_2-IDPL single crystal can obtain ambipolar transport because of its small injection barrier for both holes and electrons. Therefore, the OFETs should exhibit ambipolar transport with high hole and electron mobilities.

3. Field-Effect Characteristics of Ph_2-IDPL Film

The gas deposition method was used to fabricate OFETs with highly crystallized Ph_2-IDPL film. **Figure 3**a shows a schematic drawing of this method. Ph_2-IDPL film is deposited in a dry nitrogen atmosphere at $P_{N2} \approx 0.5$ kPa, where P_{N2} represents the partial pressure of nitrogen. The crystallinity of the Ph_2-IDPL film strongly depends on the partial pressure of nitrogen during this process, and $P_{N2} \approx 0.5$ kPa is the best condition for obtaining highly crystallized Ph_2-IDPL film.[16] The evaporation source is fixed close to the substrate ($d \approx 1$ cm). This distance is another important experimental condition for obtaining crystallized film using the gas deposition method. Figure 3b,c shows a schematic drawing and a photograph of top-contact bottom-gate OFETs, respectively, fabricated from Ph_2-IDPL film. The Ph_2-IDPL film is deposited on a self-assembled monolayer (SAM)-modified SiO_2 substrate. Hexamethyldisilazane (HMDS) SAM and phenyltrichlorosilane SAM are used to control the crystallinity of the Ph_2-IDPL film. There are four OFETs on the substrate to optimize channel width and channel length (Figure 3c).

Figures 4a,b shows an atomic force microscope (AFM) image and the X-ray diffraction (XRD) spectrum, respectively, of the Ph_2-IDPL film on HMDS SAM.[16] The AFM image shows the presence of many grains with an average size of several hundred nanometers. The corresponding XRD spectrum shows several sharp diffraction peaks. Peak assignment of the XRD pattern is based on the powder XRD pattern of Ph_2-IDPL with and without solvent.[14] These results reflect the high crystallinity of the film. Figure 4c,d shows an AFM image and the XRD spectrum of the Ph_2-IDPL film on phenyltrichlorosilane SAM. The AFM image shows the presence of both flat faces (label a) and sharp structures (label b) in the film. Grains with flat face are isolated from each other, whereas grains with sharp structures are connected together. The XRD spectrum shows two small peaks. Taken together, these results indicate that Ph_2-IDPL film on phenyltrichlorosilane SAM has lower crystallinity than Ph_2-IDPL film on HMDS SAM.

The OFETs constructed from highly crystalline Ph_2-IDPL film on HMDS SAM did not work, whereas those of low crystalline Ph_2-IDPL film on phenyltrichlorosilane SAM provided higher hole and electron mobilities ($\mu_h = 6.3 \times 10^{-3}$ cm^2 V^{-1} s^{-1}, $\mu_e = 1.1 \times 10^{-2}$ cm^2 V^{-1} s^{-1}) than those of amorphous Ph_2-IDPL film.[17] Furthermore, the OFETs of Ph_2-IDPL film on phenyltrichlorosilane SAM exhibited balanced hole and electron mobilities. These high hole and electron mobilities must be induced by formation of Ph_2-IDPL molecular chains. **Figure 5**a,b shows the p- and n-channel output characteristics of the OFET, respectively, fabricated with the Ph_2-IDPL film on phenyltrichlorosilane SAM. I_d, V_d, and V_g represent the source–drain current, source–drain voltage, and source–gate voltage, respectively. These measurements were performed in a high vacuum after the OFETs were exposed to air. Thus, Ph_2-IDPL film has chemical stability in air. The hole and electron mobilities were calculated for the saturation region ($|V_d| = 30$ V: V_d represents the source–drain voltage); the channel length is $l = 40$ μm and the channel width is $w = 1$ mm. The channel region is calculated from the channel length and channel width. Thus, a grain lager than 40 μm should exhibit fast carrier transport, while the AFM results (Figure 4a,c) show that the grains of the present film are only several micrometers long. Therefore, the electrical properties of the OFETs are affected by the grain boundaries. On the other hand, the Ph_2-IDPL film on phenyltrichlorosilane SAM exhibits lower crystallinity than that on HMDS SAM, suggesting that the effects of grain boundaries of the former are reduced due to lower crystallinity.

In addition, it is likely that the grains with sharp structures play a major role in carrier transport because grains with flat

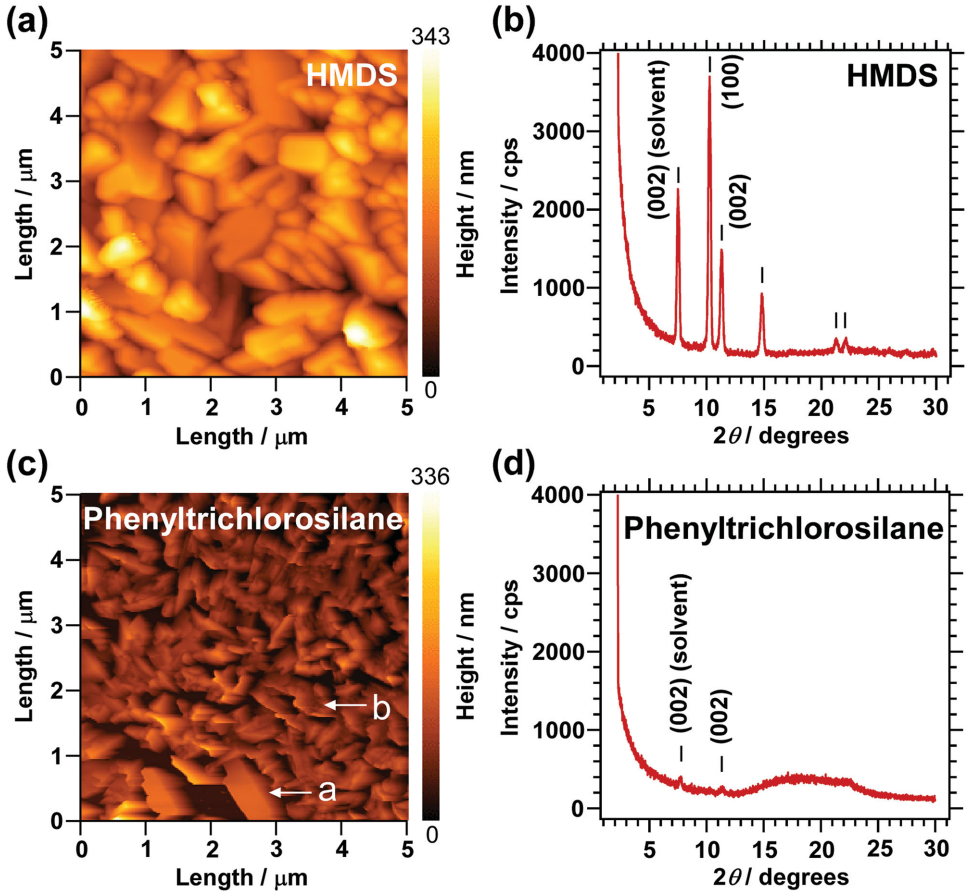

Figure 4. a) AFM image of a Ph_2-IDPL film on HMDS SAM.[16] b) XRD spectrum of a Ph_2-IDPL film on HMDS SAM.[16] c) AFM image of a Ph_2-IDPL film on phenyltrichlorosilane SAM. Labels a and b indicate grains with a flat face and with sharp structures, respectively. d) XRD spectrum of a Ph_2-IDPL film on phenyltrichlorosilane SAM.

faces are isolated from each other. Moreover, a linear I_d–V_d relationship is observed in the low V_d region in both Figures 5a,b, indicating good ohmic contact between the Au electrodes and the crystallized Ph_2-IDPL film. In the high $|V_d|$ and low $|V_g|$ regions, I_d increases after I_d is saturated. According to a theoretical study by Schmechel et al., this behavior shows that opposite carrier injection occurs at the drain electrode,[18] meaning that both holes and electrons are injected into the

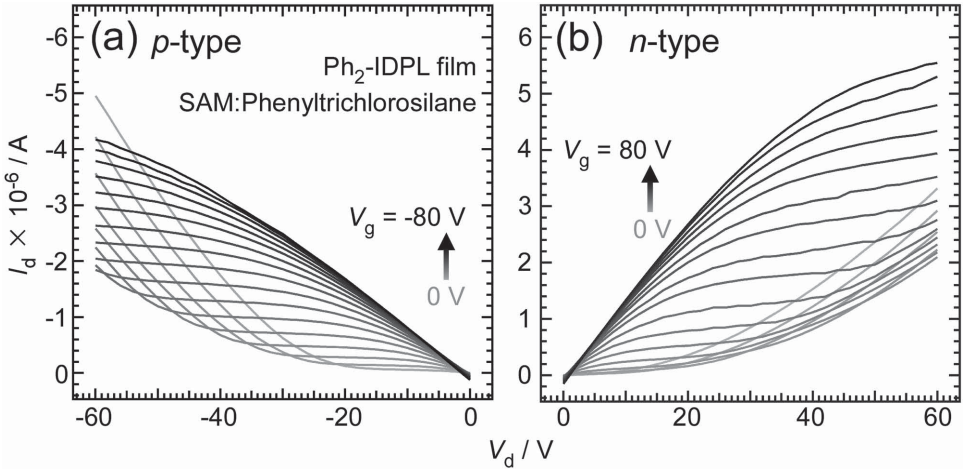

Figure 5. a) p-Channel output characteristics of an OFET with a Ph_2-IDPL film on phenyltrichlorosilane SAM. V_g was increased in –5 V increments from 0 to –80 V. b) n-Channel output characteristics of an OFET with a Ph_2-IDPL film on phenyltrichlorosilane SAM. V_g was increased in 5 V increments from 0 to 80 V.

transistor channel, resulting in balanced hole and electron mobilities.

As mentioned above, ambipolar OFETs that effectively utilize high crystallinity film could not be obtained because the crystal grain size was smaller than the channel region of the OFETs. Since carrier transport in thin films was prevented by many grain boundaries, we next fabricated Ph_2-IDPL single crystals to avoid the effect of grain boundaries and used these single crystals as the active layer in OFETs.

4. Field-Effect Characteristics of Ph_2-IDPL Single Crystals

Figure 6a,b shows a schematic drawing and a photograph, respectively, of a bottom-contact bottom-gate OFET with a Ph_2-IDPL single crystal. Ph_2-IDPL single crystals were grown by physical vapor transport technique using dry nitrogen as the carrier gas (see Figure S1 in the Supporting Information,).[19] Polarized light images allowed us to confirm that the obtained crystals are composed of a single crystalline domain (see Figure S2 in the Supporting Information). Figure 6c,d shows the p- and n-channel output characteristics, respectively, of the OFET. The channel length is $l = 1.0 \times 10$ μm and the channel width is $w = 1.11 \times 10^{-1}$ mm. The OFET shows high hole mobility ($\mu_h = 7.2 \times 10^{-1}$ cm^2 V^{-1} s^{-1}) comparable to that of amorphous Si. Hole mobility was calculated in the saturation region ($V_d = -60$ V). The OFETs with a Ph_2-IDPL single crystal show about two hundred times higher mobility than OFETs fabricated from amorphous Ph_2-IDPL film using untreated Au electrodes. This result indicates that the development of the energy band structure must lead to high hole mobility, allowing coherent carrier conduction. On the other hand, electron mobility was not observed in Figure 6d. It is likely that OH groups at the surface of neat SiO_2 work as electron traps.[20] In the high $|V_d|$ and low $|V_g|$ region in Figure 6c, I_d scarcely increases after I_d is saturated, and this indicates that only a few electrons are injected from the drain electrode.

These results show that OFETs fabricated using a Ph_2-IDPL single crystal exhibit high hole mobility comparable to that of amorphous Si. Furthermore, the hole mobility can be further improved by optimizing the orientation of Ph_2-IDPL single crystals. Consequently, delocalized singlet biradical hydrocarbon is a promising new semiconducting material for high-performance OFETs.

However, the on/off current ratio of ambipolar OFETs is generally lower than that of unipolar OFETs. The on/off current ratios of OFETs fabricated with a Ph_2-IDPL single crystal and amorphous Ph_2-IDPL film are about 57 ($V_d = -60$ V) and 10^3,[17] respectively. Although the on/off ratio of amorphous Ph_2-IDPL film is not as low as that of ambipolar OFETs fabricated using small molecules, it is much lower than that of unipolar

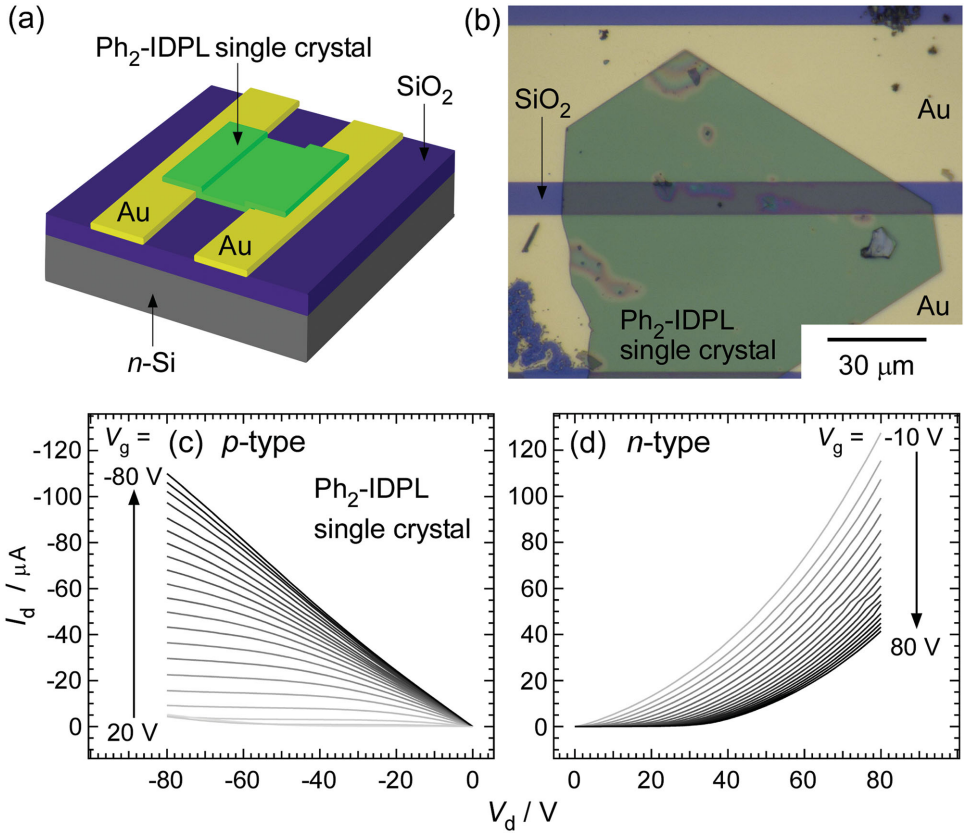

Figure 6. a) Schematic drawing of a bottom-contact bottom-gate OFET with a Ph_2-IDPL single crystal. b) Photograph of the OFET. c) p-Channel output characteristics of an OFET with a Ph_2-IDPL single crystal. V_g was increased in −5 V increments from 20 to −80 V. d) n-Type output characteristics of an OFET with a Ph_2-IDPL single crystal. V_g was increased in −5 V increments from −10 to 80 V.

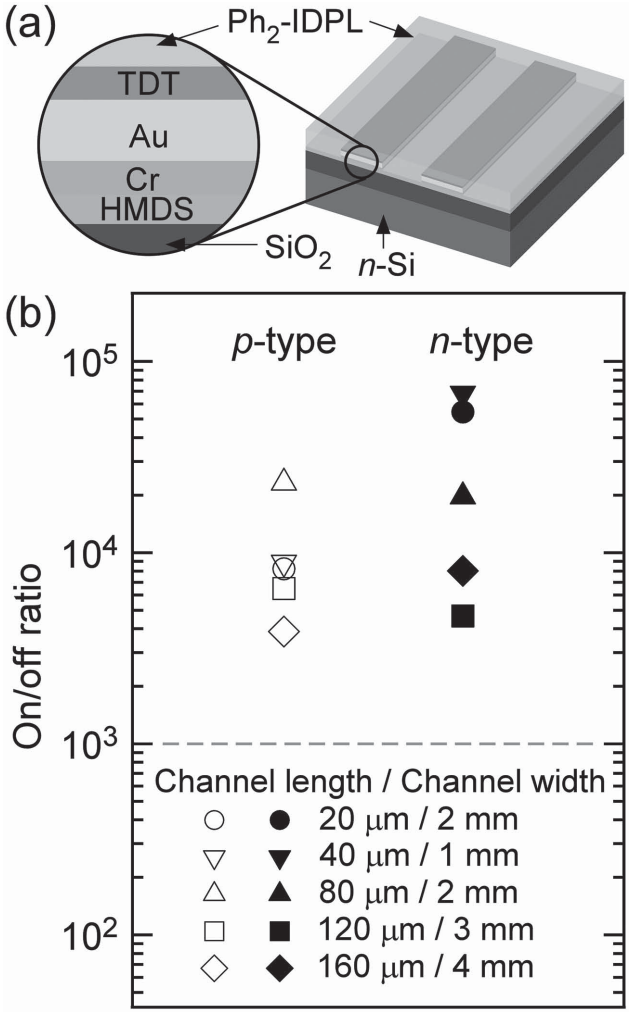

Figure 7. a) Schematic drawing of a bottom-contact bottom-gate OFET with a Ph_2-IDPL film and TDT SAM. b) On–off ratios of an OFET with different channel lengths and channel widths. Values shown are the highest value obtained with each device.

OFETs.[21–24] This low on/off ratio is caused by leakage current in OFETs in the off-state and increases the standby power; this is a longstanding problem with ambipolar OFETs. Therefore, we attempted to improve the on/off ratio of OFETs fabricated using Ph_2-IDPL.

5. Improvement of the On/Off Ratio

To reduce the leakage current in the off-state, the surfaces of the Au electrodes were treated with 1-tetradecanethiol (TDT) SAM. **Figure 7**a shows a schematic drawing of a bottom-contact bottom-gate OFET with amorphous Ph_2-IDPL film and TDT SAM. Figure 7b shows the on/off ratios; these ratios are the highest value in each device for the following channel length and channel width ratios: l/w = 20 μm/2 mm, 40 μm/1 mm, 80 μm/2 mm, 120 μm/3 mm, and 160 μm/4 mm. The p- and n-channel output characteristics of the OFETs are shown in Figure S3 in the Supporting Information. All the on/off ratios are higher than that of amorphous Ph_2-IDPL film using untreated Au electrodes (on/off ratio of about 10^3).[17] The enhanced on/off ratios result from the introduction of TDT SAM because TDT SAM dramatically reduces the off current in each device. There is no systematic trend with respect to the channel length and channel width. Thus, TDT SAM must work as a thin insulating layer. As a consequence, when the source–drain voltage is low, the source–drain current is reduced because TDT SAM prevents injection of holes and electrons. On the other hand, when the source–drain voltage is high, the source-drain current becomes larger than that in low source–drain voltage region due to tunneling transport through the insulating TDT SAM. This method can be easily applied to other OFETs with low on/off ratios. It should therefore be possible to fabricate high-performance OFETs with both high ambipolar mobility and high on/off ratio using Ph_2-IDPL single crystals in the future. This will allow the fabrication of organic logic circuits with fast switching behavior and low standby power using only one kind of ambipolar material as the active layer.

6. Conclusion

The singlet biradical nature of crystallized Ph_2-IDPL film results in development of a band structure and small HOMO–LUMO gaps. Here, we focused on the relationship between the electronic structure of the organic semiconductor and the electrical properties of the OFETs. Stable OFETs were fabricated with crystallized Ph_2-IDPL film prepared using the gas deposition method to obtain OFETs exhibiting high ambipolar mobilities. However, grain boundaries in the Ph_2-IDPL film prevented carrier transport. Highly coherent energy band transport was attained by using Ph_2-IDPL single crystals, and the OFETs fabricated using Ph_2-IDPL single crystals showed high hole mobility ($\mu_h = 7.2 \times 10^{-1}$ cm^2 V^{-1} s^{-1}) comparable to that of amorphous Si. Moreover, leakage current was reduced in the off-state and the on/off ratio was increased by using Au electrodes treated with TDT SAM. In general, ambipolar OFETs fabricated using small molecules suffer from high off current. Our results therefore open up the possibility of low-power organic logic circuits. In addition, the results indicate that strong intermolecular interactions derived from the singlet biradical nature of Ph_2-IDPL induce high mobility, and that Ph_2-IDPL holds significant promise as a new semiconducting material for high-performance organic devices.

7. Experimental Section

Material: Ph_2-IDPL was synthesized following the literature.[14]

DFT Calculations: Molecular orbital calculations were performed based on DFT using the GAUSSIAN 09 package at the PW91/6-31G* level.[25]

Fabrication of Top-Contact Bottom-Gate OFETs, Shown in Figure 3c: The top-contact bottom-gate OFETs shown in Figure 3 were fabricated on highly doped n-type Si wafer covered with 300 nm thick SiO_2 (capacitance per unit area C_i = 10 nF cm^{-2}). The SiO_2 substrates were cleaned in an ultrasonic bath for 15 min in acetone, Semico-Clean 56 (Furuuchi Chemical Corp.), hyperpure water, and then ethanol. Next, the substrates were exposed to a UV–ozone atmosphere for 20 min.

SAM was fabricated by immersing the substrates for 2 h in HMDS or phenyltrichlorosilane diluted with toluene, then the substrates were rinsed and ultrasonically cleaned in chloroform or toluene for 5 min, respectively. Next, Ph_2-IDPL was deposited on the substrates under a dry nitrogen atmosphere at $P_{N2} \approx 0.5$ kPa. The evaporation source was fixed close to the substrate ($d \approx 1$ cm). Finally, 30 nm thick Au electrodes were deposited and patterned on the substrates.

Electrical and Structural Characterization: The OFET characteristics were measured using a Keithley 4200-SCS semiconductor characterization system. Out-of-plane XRD measurements were performed in air on a Rigaku RU-300 using Cu Kα radiation (40 kV, 200 mA). AFM measurements were performed on a Seiko Instruments SPA300 in dynamic force mode under the ambient atmosphere. Polarized light microscopy was performed with a Nikon SMZ1000. Ph_2-IDPL single crystals on a quartz substrate were measured using parallel and crossed analyzer–polarizer configurations.

Fabrication of Ph_2-IDPL Single Crystals: Ph_2-IDPL single crystals were grown by physical vapor transport technique using dry nitrogen as the carrier gas (Figure S1, Supporting Information).[19] The optimum nitrogen gas flow was 50 cc min^{-1} at approximately 25 kPa. Ph_2-IDPL powder was annealed at around 450 °C. Ph_2-IDPL single crystals grew as platelets or needles. Single domains of platelet-shaped Ph_2-IDPL crystals were confirmed under a polarized light microscope in Figure S2 in the Supporting Information.

Fabrication of Bottom-Contact Bottom-Gate OFETs with Ph_2-IDPL Single Crystals, Shown in Figure 6: Ph_2-IDPL single crystals were grown by above-mentioned method (Figure S1, Supporting Information). Au electrodes were fabricated by photolithography on a SiO_2 substrate cleaned in an ultrasonic bath for 15 min in acetone, Semico-Clean 56 (Furuuchi Chemical Corp.), hyperpure water, and ethanol, and then exposed to a UV–ozone atmosphere for 20 min; this is the same cleaning method as used for cleaning substrate for the top-contact bottom-gate OFETs. Ph_2-IDPL single crystals were placed on the substrates without SAM. The channel length was $l = 1.0 \times 10$ μm and the channel width was $w = 1.11 \times 10^{-1}$ mm. w was calculated from the average value of the widths of Ph_2-IDPL single crystals on the upper electrode ($w_u = 1.05 \times 10^{-1}$ mm) and on the lower electrode ($w_l = 1.17 \times 10^{-1}$ mm) in Figure 6b.

Fabrication of Bottom-Contact Bottom-Gate OFETs with Ph_2-IDPL Film, Shown in Figure 7: The substrates were cleaned as described above. HMDS SAM was formed on the substrates, then 1 nm of Cr followed by 30 nm of Au was deposited and patterned on the substrates to fabricate Au electrodes. The substrates were immersed in TDT solution (1×10^{-3} mol L^{-1} in ethanol) for 2 h to form TDT SAM on the Au electrodes. Finally, Ph_2-IDPL was deposited on the substrates in vacuum at a deposition rate of about 0.05 Å s^{-1} to a thickness of 40–100 nm.

Supporting Information

Supporting Information is available from the Wiley Online Library or from the author.

Acknowledgements

This work was supported by a Grant-in-Aid for Scientific Research (Grant No. 24350013) from the Ministry of Education, Culture, Sports, Science and Technology of Japan (MEXT). One of the authors (H.K.) thanks Prof. M. Tamura for helpful discussions.

Received: August 28, 2015
Revised: October 9, 2015
Published online: December 2, 2015

[1] J. Takeya, M. Yamagishi, Y. Tominari, R. Hirahara, Y. Nakazawa, T. Nishikawa, T. Kawase, T. Shimoda, S. Ogawa, *Appl. Phys. Lett.* **2007**, *90*, 102120.
[2] V. Y. Butko, X. Chi, D. V. Lang, A. P. Ramirez, *Appl. Phys. Lett.* **2003**, *83*, 4773.
[3] B. Elmer, O. Schlemper, D. Britton, *Acta. Cryst.* **1965**, *18*, 419.
[4] J. D. Wright, *Molecular Crystals*, Cambridge University Press, Cambridge, UK **1995**.
[5] Y. Yamashita, S. Tanaka, K. Imaeda, H. Inokuchi, M. Sano, *J. Org. Chem.* **1992**, *57*, 20.
[6] K. Imaeda, Y. Yamashita, Y. Li, T. Mori, H. Inokuchi, M. Sano, *J. Mater. Chem.* **1992**, *2*, 115.
[7] T. Kubo, M. Sakamoto, M. Akabane, Y. Fujiwara, K. Yamamoto, M. Akita, K. Inoue, T. Takui, K. Nakasuji, *Angew. Chem.* **2004**, *116*, 6636.
[8] T. Kubo, A. Shimizu, M. Uruichi, K. Yakushi, M. Nakano, D. Shiomi, K. Sato, T. Takui, Y. Morita, K. Nakasuji, *Org. Lett.* **2007**, *9*, 81.
[9] A. Shimizu, T. Kubo, M. Uruichi, K. Yakushi, M. Nakano, D. Shiomi, K. Sato, T. Takui, Y. Hirao, K. Matsumoto, H. Kurata, Y. Morita, K. Nakasuji, *J. Am. Chem. Soc.* **2010**, *132*, 14421.
[10] Z. Sun, K. W. Huang, J. Wu, *J. Am. Chem. Soc.* **2011**, *133*, 11896.
[11] Y. Li, W. K. Heng, B. S. Lee, N. Aratani, J. L. Zafra, N. Bao, R. Lee, Y. M. Sung, Z. Sun, K. W. Huang, R. D. Webster, J. T. L. Navarrete, D. Kim, A. Osuka, J. Casado, J. Ding, J. Wu, *J. Am. Chem. Soc.* **2012**, *134*, 14913.
[12] A. Shimizu, Y. Hirao, K. Matsumoto, H. Kurata, T. Kubo, M. Uruichi, K. Yakushi, *Chem. Commun.* **2012**, *48*, 5629.
[13] A. Shimizu, R. Kishi, M. Nakano, D. Shiomi, K. Sato, T. Takui, I. Hisaki, M. Miyata, Y. Tobe, *Angew. Chem.* **2013**, *125*, 6192.
[14] T. Kubo, A. Shimizu, M. Sakamoto, M. Uruichi, K. Yakushi, M. Nakano, D. Shiomi, K. Sato, T. Takui, Y. Morita, K. Nakasuji, *Angew. Chem. Int. Ed.* **2005**, *44*, 6564.
[15] K. Kanai, Y. Noda, K. Kato, T. Kubo, K. Iketaki, A. Shimizu, Y. Ouchi, K. Nakasuji, K. Seki, *Phys. Chem. Chem. Phys.* **2010**, *12*, 12570.
[16] H. Koike, T. Kubo, K. Uchida, M. Chikamatsu, R. Azumi, K. Mase, K. Kanai, *Appl. Phys. Lett.* **2013**, *102*, 134103.
[17] M. Chikamatsu, T. Mikami, J. Chisaka, Y. Yoshida, R. Azumi, K. Yase, A. Shimizu, T. Kubo, Y. Morita, K. Nakasuji, *Appl. Phys. Lett.* **2007**, *91*, 043506.
[18] R. Schmechel, M. Ahles, H. V. Seggern, *J. Appl. Phys.* **2005**, *98*, 084511.
[19] Ch. Kloc, P. G. Simpkins, T. Siegrist, R. A. Laudise, *J. Cryst. Growth* **1997**, *182*, 416.
[20] L. L. Chua, J. Zaumseil, J. F. Chang, E. C. W. Ou, P. K. H. Ho, H. Sirringhaus, R. H. Friend, *Nature* **2005**, *434*, 194.
[21] Y. Sakamoto, T. Suzuki, M. Kobayashi, Y. Gao, Y. Fukai, Y. Inoue, F. Sato, S. Tokito, *J. Am. Chem. Soc.* **2004**, *126*, 8138.
[22] T. Yasuda, T. Tsutsui, *Chem. Phys. Lett.* **2005**, *402*, 395.
[23] R. J. Chesterfield, C. R. Newman, T. M. Pappenfus, P. C. Ewbank, M. H. Haukaas, K. R. Mann, L. L. Miller, C. D. Frisbie, *Adv. Mater.* **2003**, *15*, 15.
[24] D. He, Y. Zhang, Q. Wu, R. Xu, H. Nan, J. Liu, J. Yao, Z. Wang, A. Yuan, Y. Li, Y. Shi, J. Wang, Z. Ni, L. He, F. Miao, F. Song, H. Xu, K. Watanabe, T. Taniguchi, J. B. Xu, X. Wang, *Nat. Commun.* **2014**, *5*, 5162.
[25] M. J. Frisch, G. W. Trucks, H. B. Schlegel, G. E. Scuseria, M. A. Robb, J. R. Cheeseman, G. Scalmani, V. Barone, B. Mennucci, G. A. Petersson, H. Nakatsuji, M. Caricato, X. Li, H. P. Hratchian, A. F. Izmaylov, J. Bloino, G. Zheng, J. L. Sonnenberg, M. Hada, M. Ehara, K. Toyota, R. Fukuda, J. Hasegawa, M. Ishida, T. Nakajima, Y. Honda, O. Kitao, H. Nakai, T. Vreven, J. A. Montgomery Jr., J. E. Peralta, F. Ogliaro, M. Bearpark, J. J. Heyd, E. Brothers, K. N. Kudin, V. N. Staroverov, T. Keith, R. Kobayashi, J. Normand, K. Raghavachari, A. Rendell, J. C. Burant, S. S. Iyengar, J. Tomasi, M. Cossi, N. Rega, J. M. Millam, M. Klene, J. E. Knox, J. B. Cross, V. Bakken, C. Adamo, J. Jaramillo, R. Gomperts, R. E. Stratmann, O. Yazyev, A. J. Austin, R. Cammi, C. Pomelli, J. W. Ochterski, R. L. Martin, K. Morokuma, V. G. Zakrzewski, G. A. Voth, P. Salvador, J. J. Dannenberg, S. Dapprich, A. D. Daniels, O. Farkas, J. B. Foresman, J. V. Ortiz, J. Cioslowski, D. J. Fox, *Gaussian 09 B. 01*, Gaussian, Inc., Wallingford, CT, USA **2010**.